Received 24 December 2017
Revised 20 February 2018
Accepted 14 March 2018

Effect of radiation absorption and buoyancy force on the MHD mixed convection flow of Casson nanofluid embedded with $Al_{50}Cu_{50}$ alloy nanoparticles

G.P. Ashwinkumar
Department of Mathematics, Gulbarga University, Gulbarga, India and Department of Mathematics, SP and JMB Degree College, Shorapur, India, and
Sulochana C.
Department of Mathematics, Gulbarga University, Gulbarga, India

Abstract

Purpose – The purpose of this paper is to report the effects of radiation absorption and buoyancy forces on the boundary layer analysis of Casson nanofluid past a vertical plate in a porous enclosure filled with $Al_{50}Cu_{50}$ alloy nanoparticles.

Design/methodology/approach – The authors reconstructed the controlling equations as a group of nonlinear ODEs and solved analytically using perturbation technique. The vital interest in this analysis is to examine the influence of sundry physical parameters on the common profiles (velocity, temperature and concentration) conferred through the plots. Tabular values are listed to discuss the skin friction factor, heat and mass transfer rates. Dual solutions are observed for Newtonian and non-Newtonian fluid cases.

Findings – Acquired results indicate that the Casson fluid plays a major role in controlling heat and mass transfer rates as compared with Newtonian fluid. Also, raise in volume fraction of nanoparticles regulates the thermal fields, discerns the velocity fields. The authors established the comparison of present results with previously published results and they are found in good agreement for limited cases.

Originality/value – Because of the substantial properties of aluminium and its alloys such as, extreme corrosion resistance, exalted electrical and thermal conductivities and ease of fabrication they achieved tremendous applications in transportation especially in space and aircrafts, in the production of electrical transmission lines. In view of these, the current literature is perpetrated to probe the impact of radiation absorption and buoyancy forces on the heat and mass transfer analysis of Casson nanofluid in the presence of $Al_{50}Cu_{50}$ alloy nanoparticles.

Keywords Nanofluid, Chemical reaction, Radiation absorption, Casson model, Viscous dissipation

Paper type Research paper

Nomenclature

x,y	Cartesian coordinates (m)	C_∞	ambient concentration
u,v	velocity component at x, y direction, respectively (ms^{-1})	Ec	viscous dissipation parameter
		D_B	molecular diffusivity
T	fluid temperature (K)	Sc	Schmidt number
V_0	constant suction velocity	R_d	radiation parameter
T_w	free stream temperature (K)	K	porosity parameter
T_∞	ambient temperature	K_r	chemical reaction parameter
C_w	free stream concentration	Gt	thermal Grashof number

The authors would like to thank the competent anonymous referees for their valuable comments and suggestions. The first author acknowledges the UGC for financial support under the UGC Rajiv Gandhi National Fellowship for Scheduled Caste Students (RGNFSC) Scheme (No. F1-17.1/2017-18/RGNF-2017-18-SC-KAR-36100).

Multidiscipline Modeling in Materials and Structures
Vol. 14 No. 5, 2018
pp. 1082-1100

1573-6105
DOI 10.1108/MMMS-12-2017-0164

Gc	concentration Grashof number
Pr	Prandtl number
Q_0	heat source/sink parameter
Q_1	radiation absorption parameter
C_{fx}	skin friction coefficient
k^*	mean absorption coefficient
k	thermal conductivity (W/mK)
q_w	heat flux from the flux ($Jm^{-2}s^{-1)}$
Nu_x	local Nusselt number
Rex	local Reynolds number

Greek symbols

ρ_{nf}	effective density of the Casson nanofluid (kgm^{-3})
μ_{nf}	dynamic viscosity of the Casson nanofluid ($kgm^{-1}s^{-2}$)
$(\rho c_p)_{nf}$	heat capacitance of nanofluid ($Jm^{-3}K^{-1}$)
k_{nf}	thermal conductivity of the nanofluid
ρ_f	density of the base fluid (kgm^{-3})
ρ_s	density of the solid particle (kgm^{-3})
k_f	thermal conductivity of base fluid
ξ	Casson Parameter
Φ	solid volume fraction of nanoparticle
υ_f	kinematic viscosity of the fluid (m^2/s)
θ	dimensionless temperature
ζ	dimensionless concentration

Subscripts

nf	nanofluid
f	base fluid

1. Introduction

In modern days the boundary layer analysis on the flow of non-Newtonian fluids has fascinated the research community because of the large practical applications in engineering and industries such as chemical industries, mechanical engineering, thermal insulation, biochemical process, food process, etc. Non-Newtonian fluid possesses more viscosity and highly nonlinear governing equations than Newtonian fluid. Casson fluid is one of the type of non-Newtonian fluids, the non-Newtonian fluid behaviour described with the yield stress, whose flow rate is not directly proportional to the strain rate. Pham and Mitsoulis (1994) elaborated the use of Casson fluid model in describing the blood flow. Wang and Pop (2006) deliberated the heat transfer analysis of non-Newtonian fluid caused by stretching surface using Homotopy analysis method. Tso *et al.* (2010) discussed the influence of frictional heating effects on the flow of non-Newtonian fluid past parallel plates with constant heat flux. The flow and heat transfer analysis of Casson fluid past nonlinear stretched surface was studied by Mukhopadhyay (2013). The author noticed that improvement in values of nonlinear stretching parameter reduces the fluid velocity. Shehzad *et al.* (2013) conversed the mass transfer analysis on the flow of Casson fluid in the presence of chemical reaction parameter. Pramanik (2014) studied the impact of thermal radiation on the boundary layer analysis of Casson fluid past an exponential porous distending surface, they perceived that thermal diffusivity enhances as the radiation value improves. Ibrahim and Makinde (2015) elaborated the stagnation-point flow of Casson fluid past elongated surface with slip and convective boundary conditions. Later, few researchers (Raju and Sandeep, 2016; Mahdy, 2016; Sulochana *et al.*, 2016; Raju and Sandeep, 2017; Kumaran and Sandeep, 2017) explained the boundary layer analysis of Casson fluid past various geometries such as a wedge, elongated surface, vertical oscillating plate, rotating cone, thin film, paraboloid of revolution in the presence of different physical parameters. Recently, Sulochana *et al.* (2017b) deliberated the influence of frictional heating on the radiative Casson fluid over an inclined plate immersed in the porous medium.

The conventional fluids such as water, kerosene, oils, methanol used in industrial applications, they found a drawback of possessing lower thermal conductivity. To overcome this drawback the industrialists and researchers are fascinated towards the new class of technology named as nano-technology. Nanofluids are the dispersal of solid nanomaterials such as Al, Cu, TiO_2, $Al_{50}Cu_{50}$, Fe_3O_4, etc. of size ranges between 1 and 100 nanometres in the conventional fluids. These fluids are mainly synthesised

to attain enormous thermal conductivity as compared with any other liquids. Nano-technology was initially incorporated by Choi (1995) to enhance the heat transfer performance of base fluids. Later, Buongiorno (2006) employed seven slip mechanism to upsurge the thermal conductivity of base liquids by means of adding nanometre scaled solid particles, he found that out of seven slip mechanism Brownian diffusion and thermophoresis play vital role in improving thermal conductivity. Nield and Kuznetsov (2009) extended the Chenge Minkowycz problem to the nanofluid case. Vajravelu *et al.* (2011) utilised the Silver-water and Copper-water nanofluids over an elongated surface. Ibrahim and Shankar (2013) examined the flow of nanofluid past elongated surface in the presence of velocity, thermal and solutal boundary conditions. Further Dogonchi and Ganji (2017a, b, 2016a, b, c) provided the detailed studies on the impact of Joule heating, Cattaneo-Christov heat flux, Brownian motion, thermal radiation on the heat and mass transfer characteristics of nanofluid flows past various geometries.

Moreover, the boundary layer analysis of non-Newtonian nanofluid past stretched surface with external magnetic field effects was discussed by Madhu and Kishan (2015). Later Sandeep and Sulochana (2016) examined the flow of dusty nanofluid past elongated surface in the presence of an external magnetic field, they studied the boundary layer analysis for fluid phase and dust phase cases. Daniel and Daniel (2015) discussed the effect of buoyancy and thermal radiation on the MHD flow past elongated porous sheet using homotopy analysis solution. Babu and Sandeep (2016) studied the 3D slip flow of nanofluids past distending surface in the presence of thermophoresis and Brownian motion effects, they perceived that heat and mass transfer performance of Cu-water nanofluid is more as compared with CuO-water nanofluid. Raju *et al.* (2016) discussed the 3D flow of nanofluid past an elongated surface in the presence of an external magnetic field, they perceived dual solutions. Sulochana *et al.* (2017c, d) incorporated the Buongiorno (2006) slip mechanisms in the analysis of enhancing the thermal conductivity of the conventional fluids. Recently, Babu *et al.* (2017) deliberated the MHD flow over a slendering stretching surface. They obtained the enhanced heat and mass transfer rates for rising values of thickness parameter. Daniel *et al.* (2017a, b, c) analysed the impact of thermal radiation, viscous dissipation, Joule heating on the flow of nanofluid past an elongated sheet. Very recently, Sulochana *et al.* (2017a) discussed numerically the boundary layer analysis of magnetic nanofluid flow caused by thin needle. They found that heat transfer performance of methanol-based ferrofluid is large when compared with water-based ferrofluid for rising values of volume fraction parameters. Daniel (2017) adopted partial slip conditions in their analysis of flow and heat transfer behaviour of viscous fluid past stretching sheet.

Motivated by aforementioned findings, we filled the gap by extending the work of Pal and Talukdar (2010). The novelty of the study is to discuss the heat and mass transfer characteristics of Casson nanofluid in the presence of thermal radiation and chemical reaction effects. We pondered perturbation technique to solve the ODEs and with the aid of Matlab software we bestowed the plots and numerical values. The impact of various physical parameters on velocity, thermal and concentration attributes are deployed with the succour of graphs. For practical interest, we conversed the impact of aforesaid parameters on skin friction factor, local Nusselt number and Sherwood number and are deployed in tabular forms. Dual nature is observed for the Newtonian fluid and non-Newtonian fluid cases.

2. Mathematical formulation

We presume the viscous, incompressible 2D boundary layer flow of Newtonian and non-Newtonian nanofluid over a permeable semi-infinite vertical plate immersed in a porous

medium, under the consideration of thermal and concentration buoyancy effects and dissipation effects the flow model is shown in Figure 1.

The plate is placed along the x-axis and it is perpendicular to the y-axis. Here T_w and C_w are the constant temperature and concentration applied at the wall which is higher than T_∞ and C_∞. Where T_∞ and C_∞ are the ambient temperature and concentration, respectively. It is also noticed that thermal radiation and chemical reaction effects are taken into consideration. And also to make our study unique we introduced the concept of suspension of $Al_{50}Cu_{50}$ Alloy nanoparticles into the base liquid. Under the presence of above physical assumptions, as the flow governing equations are stated by Pal and Talukdar (2010) are reduced as below:

$$\frac{\partial v}{\partial y} = 0 \Rightarrow v' = -V_0, \tag{1}$$

$$\rho_{nf}\left(v^*\frac{\partial u^*}{\partial y^*}\right) = \mu_{nf}\left(1+\xi^{-1}\right)\frac{\partial^2 u^*}{\partial y^{*2}} - \frac{\mu_{nf}}{k^*}u^* + (\rho\beta)_{nf}\left(g\left(T^*-T_\infty\right)+g\left(C^*-C_\infty\right)\right), \tag{2}$$

$$\left(\rho c_p\right)_{nf}\left(v^*\frac{\partial T^*}{\partial y^*}\right) = k_{nf}\frac{\partial^2 T^*}{\partial y^{*2}} + \mu_{nf}\left(1+\xi^{-1}\right)\left(\frac{\partial u^*}{\partial y^*}\right)^2 - \frac{\partial q_r}{\partial y^*} - Q_0^*\left(T^*-T_\infty\right) + Q_1^*\left(C^*-C_\infty\right), \tag{3}$$

$$v^*\frac{\partial C^*}{\partial y^*} = D_B\left(\frac{\partial^2 C^*}{\partial y^{*2}}\right) - H\left(C^*-C_\infty\right), \tag{4}$$

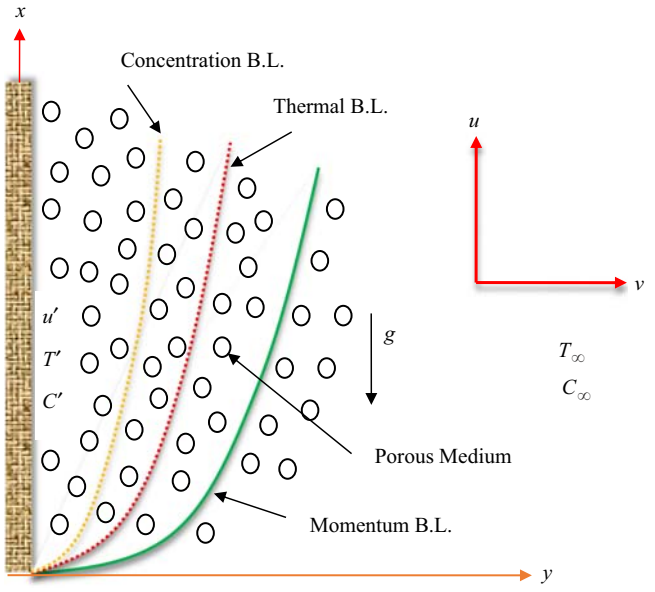

Figure 1.
Flow geometry of the problem

where u and v are the velocity towards the x and y axes, respectively. And $\phi, \rho_{nf}, \mu_{nf}, (\rho c_p)_{nf}, k_{nf}$ are the volume fraction, effective density, effective dynamic viscosity, heat capacitance and thermal conductivity of the nanofluid which are stated as follows:

$$\rho_{nf} = \rho_f(1-\varphi)+\varphi\rho_s, \tag{5}$$

$$\mu_{nf} = \mu_f(1-\varphi)^{-2.5}, \tag{6}$$

$$(\rho c_p)_{nf} = (\rho c_p)_f(1-\varphi)+\varphi(\rho c_p)_s, \tag{7}$$

$$k_{nf} = k_f\left(\frac{k_s+2k_f-2\phi(k_f-k_s)}{k_s+2k_f+2\phi(k_f-k_s)}\right). \tag{8}$$

The radiative heat flux is given by:

$$\frac{\partial q_r}{\partial y'} = 4(T'-T_\infty)L^{\cdot}, \tag{9}$$

where $L^{\cdot} = \int_0^\infty K_{\lambda w}(\partial e_{b\lambda}/\partial T')d\lambda_{,}$, $K_{\lambda w}$ is the absorption coefficient at the wall and $e_{b\lambda}$ is Plank's function.

The rheological equation of a Casson fluid is given by:

$$\tau_{ij} = \begin{cases} 2(\mu_B+p_y/\sqrt{2\pi})e_{ij}, & \pi > \pi_c \\ 2(\mu_B+p_y/\sqrt{2\pi})e_{ij}, & \pi < \pi_c \end{cases} \tag{10}$$

The related boundary conditions are:

$$u^* = 0, \quad T^* = T_\infty, \quad C^* = C_\infty, \quad \text{at } y = 0$$

$$u^* \to 0, \quad T^* \to T_\infty, \quad C^* \to C_\infty, \quad \text{as } y \to \infty\}, \tag{11}$$

Now utilising the suitable transmutations:

$$u = \frac{u^*}{V_0}, y = \frac{V_0 y^*}{\upsilon_f}, \theta = \frac{(T^*-T_\infty)}{(T_w-T_\infty)}, \zeta = \frac{(C^*-C_\infty)}{(C_w-C_\infty)}, K = \frac{k^* V_0^2}{\upsilon_f^2}, \tag{12}$$

Using Equations (5)–(11) in basic Equations (2)–(4) reduces to the dimensionless form:

$$\left.\begin{aligned} &(1+\xi^{-1})(1-\varphi)^{-2.5}\tfrac{\partial^2 u}{\partial y^2}+\{1-\varphi+\varphi(\rho_s/\rho_f)\}\tfrac{\partial u}{\partial y}-\left\{\tfrac{(1-\varphi)^{2.5}}{K}\right\}u = \\ &-(1-\varphi+\varphi(\rho\beta_s/\rho\beta_f))\{Gt\theta-Gc\zeta\}, \end{aligned}\right\} \tag{13}$$

$$\frac{k_{nf}}{k_f}\frac{\partial^2\theta}{\partial y^2}+\Pr\left\{1-\varphi+\varphi\frac{(\rho c_p)_s}{(\rho c_p)_f}\right\}\frac{\partial\theta}{\partial y}-\Pr(R_d+Q_0)\theta = -\Pr\frac{(1+\xi^{-1})}{(1-\varphi)^{5/2}}Ec\left(\frac{\partial u}{\partial y}\right)^2-\Pr Q_1\zeta, \tag{14}$$

$$\frac{\partial^2\zeta}{\partial y^2}+Sc\frac{\partial\zeta}{\partial y}-ScK_r\zeta=0, \tag{15}$$

where Gt, Gc, Pr, ξ, Ec, K_r, R_d, Q_0, Q_1, S_c, K, φ, are thermal Grashof number, concentration Grashof number, Prandtl number, Casson parameter, Eckert number, Chemical reaction, thermal radiation, heat source/sink, radiation absorption, Schmidth number, porosity parameter and volume fraction of nanoparticles the are stated as follows:

$$\left.\begin{array}{l} Gt=\frac{(\rho\beta)_f g(T_W-T_\infty)v_f^2}{V_0^3\mu_f},\ Gc=\frac{(\rho\beta)_f g(C_W-C_\infty)v_f^2}{V_0^3\mu_f},\ \mathrm{Pr}=\frac{\mu_f c_{p_f}}{k_f},\ \xi=\mu_B\sqrt{2\pi_c}/p_y,\ Sc=\frac{v_f}{D_B} \\ Ec=\frac{V_0^2}{c_p(T_w-T_\infty)},\ K_r=\frac{Hv_f}{V_0^2},\ R_d=\frac{4v_fL'}{(\rho c_p)_f V_0^2},\ Q_0=\frac{Q_0^*v_f}{(\rho c_p)_f V_0^2},\ Q_1=\frac{Q_1^*(C_W-C_\infty)v_f}{(T_W-T_\infty)(\rho c_p)_f V_0^2} \end{array}\right\}. \tag{16}$$

The corresponding transformed boundary conditions are given by:

$$\left.\begin{array}{l} u=0,\ \theta=1,\ \psi=1\ \text{at}\ y=0 \\ u\to 0,\ \theta\to 1,\ \psi\to 1\ \text{as}\ y\to\infty \end{array}\right\} \tag{17}$$

3. Analytical solution of the problem

The Equations (13)–(15) are reduced to simplified form as below:

$$A_1u''+A_2u'-A_3u=-A_4Gt\theta-A_4Gc\zeta, \tag{18}$$

$$A_6\theta''+A_7\theta'-A_8\theta=-A_9(u')^2-A_{10}\zeta, \tag{19}$$

$$\zeta''+A_{11}\zeta'-A_{12}\zeta=0. \tag{20}$$

The set of Equations (18)–(20) are solved analytically after reducing them into ODEs. The perturbed expressions are shown below:

$$u(y)=u_0(y)+Ecu_1(y)+O\left(Ec^2\right), \tag{21}$$

$$\theta(y)=\theta_0(y)+Ec\theta_1(y)+O\left(Ec^2\right), \tag{22}$$

$$\zeta(y)=\zeta_0(y)+Ec\zeta_1(y)+O\left(Ec^2\right). \tag{23}$$

Substituting Equations (21)–(23) in Equations (18)–(20) and equating the coefficients of $Ec$to Zero-order, we get:

$$A_1u_0''+A_2u_0'-A_3u_0=-A_{44}\theta_0-A_{55}\zeta_0, \tag{24}$$

$$A_6\theta_0''+A_7\theta_0'-A_8\theta_0=-A_{10}\zeta_0, \tag{25}$$

$$\zeta_0'' + A_{11}\zeta_0' - A_{12}\zeta_0 = 0, \tag{26}$$

Equating the coefficients of Eckert number to first order we get:

$$A_1 u_1'' + A_2 u_1' - A_3 u_1 = -A_{44}\theta_1 - A_{55}\zeta_1, \tag{27}$$

$$A_6\theta_1'' + A_7\theta_1' - A_8\theta_1 = -A_9\left(u_0'\right)^2 - A_{10}\zeta_1, \tag{28}$$

$$\zeta_1'' + A_{11}\zeta_1' - A_{12}\zeta_1 = 0, \tag{29}$$

where "prime" denotes the ordinary differentiation w.r.t. "y".

The corresponding boundary conditions are:

$$\left.\begin{array}{lll} u_0 = 0, & \theta_0 = 1, & \psi_0 = 1 \\ u_1 \to 0, & \theta_1 \to 1, & \psi_1 \to 1 \end{array}\right\} \text{ and } \left.\begin{array}{lll} u_0 = 0, & \theta_0 = 0, & \psi_0 = 0 \\ u_1 \to 0, & \theta_1 \to 0, & \psi_1 \to 0 \end{array}\right\} as \quad y \to \infty. \tag{30}$$

Using the boundary conditions (30), the solutions of the Equations (24)–(29) we obtain the followings:

$$u_0(y) = A_{19}e^{-B_3 y} - A_{17}e^{-B_2 y} - A_{18}e^{-B_1 y}, \tag{31}$$

$$\theta_0(y) = A_{14}e^{-B_2 y} - A_{13}e^{-B_1 y}, \tag{32}$$

$$\zeta_0(y) = e^{-B_1 y}, \tag{33}$$

$$u_1(y) = B_{14}e^{-B_1 y} - B_7 e^{-B_2 y} + B_8 e^{-2B_3 y} + B_9 e^{-2B_2 y} + B_{10}e^{-2B_1 y} - B_{11}e^{-B_4 y} + B_{12}e^{-B_5 y} - B_{13}e^{-B_6 y}, \tag{34}$$

$$\theta_1(y) = A_{41}e^{-B_2 y} - A_{35}e^{-2B_3 y} - A_{36}e^{-2B_2 y} - A_{37}e^{-2B_1 y} + A_{38}e^{-B_4 y} - A_{39}e^{-B_5 y} + A_{40}e^{-B_6 y}, \tag{35}$$

$$\zeta_1(y) = 0. \tag{36}$$

Substituting the above solutions (31)–(36) in Equations (21)–(23), we get the final form of solutions for velocity, temperature and concentration as given below:

$$\left.\begin{array}{l} u(y) = \left\{\left(A_{19}e^{-B_3 y} - A_{17}e^{-B_2 y} - A_{18}e^{-B_1 y}\right) + Ec\left(B_{14}e^{-B_1 y} - B_7 e^{-B_2 y} + B_8 e^{-2B_3 y} + B_9 e^{-2B_2 y}\right.\right. \\ \left.\left. + B_{10}e^{-2B_1 y} - B_{11}e^{-B_4 y} + B_{12}e^{-B_5 y} - B_{13}e^{-B_6 y}\right)\right\} \end{array}\right\}, \tag{37}$$

$$\left.\begin{array}{l} \theta(y) = \left\{\left(A_{14}e^{-B_2 y} - A_{13}e^{-B_1 y}\right) + Ec\left(A_{41}e^{-B_2 y} - A_{35}e^{-2B_3 y} - A_{36}e^{-2B_2 y} - A_{37}e^{-2B_1 y}\right.\right. \\ \left.\left. + A_{38}e^{-B_4 y} - A_{39}e^{-B_5 y} + A_{40}e^{-B_6 y}\right)\right\} \end{array}\right\}, \tag{38}$$

$$\zeta(y) = e^{-B_1 y}. \tag{39}$$

The physical quantities of practical interest are wall friction; local Nusselt number and local Sherwood number are given as follows.

Wall shear stress τ_w is given as:

$$\tau_w = \mu \left.\frac{\partial u^*}{\partial y^*}\right|_{y^*=0} = \rho_f V_0^2 u_0'(0). \tag{40}$$

The friction factor is given as:

$$\left.\begin{aligned} C_{fx} = \frac{\tau_w}{\rho_f V_0^2} = u'(0) = \{&(-B_3A_{19} + B_2A_{17} + B_1A_{18}) + Ec(-B_1B_{14} + B_2B_7 - 2B_3B_8 \\ &-2B_2B_9 - 2B_1B_{10} + B_4B_{11} - B_5B_{12} + B_6B_{13})\} \end{aligned}\right\}. \tag{41}$$

The local surface heat flux is given as:

$$q_w = -k \left.\frac{\partial T^*}{\partial y^*}\right|_{y^*=0}. \tag{42}$$

The local Nusselt number is given as:

$$Nu_x = \frac{q_w}{(T_w - T\infty)}, \tag{43}$$

$$\left.\begin{aligned} \frac{Nu_x}{\mathrm{Re}_x} = -\left.\frac{\partial\theta}{\partial y}\right|_{y=0} = -\theta'(0) = -\{&(-B_2A_{14} + B_1A_{13}) + Ec(-B_2A_{14} + 2B_3A_{35} + 2B_2A_{36} \\ &+2B_1A_{37} - B_4A_{38} + B_5A_{39} - B_6A_{40})\} \end{aligned}\right\}. \tag{44}$$

The local Sherwood number is given as:

$$\frac{Sh_x}{\mathrm{Re}_x} = -\left.\frac{\partial\zeta}{\partial y}\right|_{y=0} = -\zeta'(0) = -B_1, \tag{45}$$

where $\mathrm{Re}_x = V_0 x/\upsilon_f$ is the local Reynolds number.

4. Analysis of the results

In this section we discuss the impact of various physical parameters such as Prandtl number, thermal Grashof number, concentration Grashof number, volume fraction of nanoparticles, thermal radiation, chemical reaction, heat source, radiation absorption parameter on the flow quantities, namely velocity, thermal and concentration attributes of $Al_{50}Cu_{50}$-water nanofluid along with skin friction, local Nusselt and Sherwood number for both the Newtonian and non-Newtonian fluid cases using graphical notions and tabular forms. The system of nonlinear ODEs (13) to (15) with corresponding boundary restrictions (16) are solved analytically by using simple perturbation technique. We assumed the following values of physical parameters in the analysis $R_d = 3$; $Gt = 4.0$; $Gc = 2.0$; $Q_0 = 2.0$; $Q_1 = 2.0$; $\mathrm{Pr} = 0.7$; $Sc = 0.6$; $Ec = 0.01$; $\varphi = 0.05$; $\xi = 0.5$; $K_r = 0.1$; $K = 0.5$;. These values are invariant unless otherwise specified in the tables and figures.

Figures 2 and 3 depicts the impact of improving values of the volume fraction of nanoparticles over a velocity and thermal distributions. It is evident that raising the volume fraction of nanoparticles suppress the fluid velocity, in turn, it develops the temperature. Raising the magnitude of nanoparticle improves solidity of nanofluid which leads to augment thermal profile and also curtails the stream velocity. It is also observed that Casson fluid moves more rapidly than Newtonian fluid. Figures 4 and 5 deployed to analyse the effect of thermal Grashof number and concentration Grashof over velocity curves, respectively.

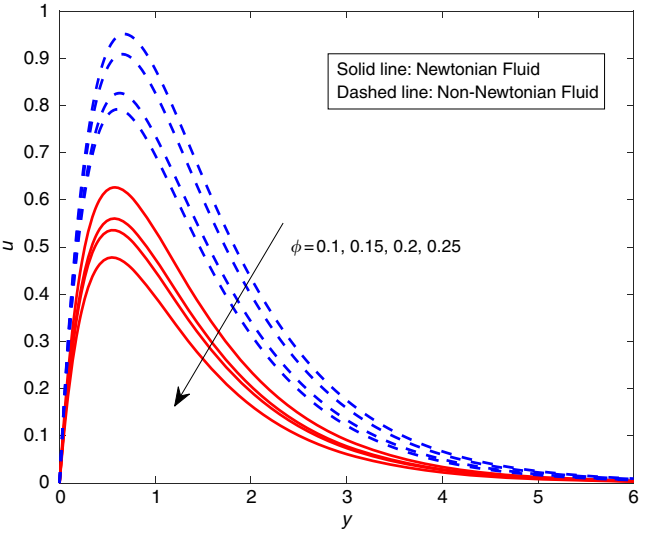

Figure 2.
Effect of φ on velocity distributions for $R_d = 3$; $Gt = 4.0$; $Gc = 2.0$; $Q_0 = 2.0$; $Q_1 = 2.0$; Pr = 0.7; $Sc = 0.6$; $Ec = 0.01$; $\xi = 0.5$; $K_r = 0.1$; $K = 0.5$

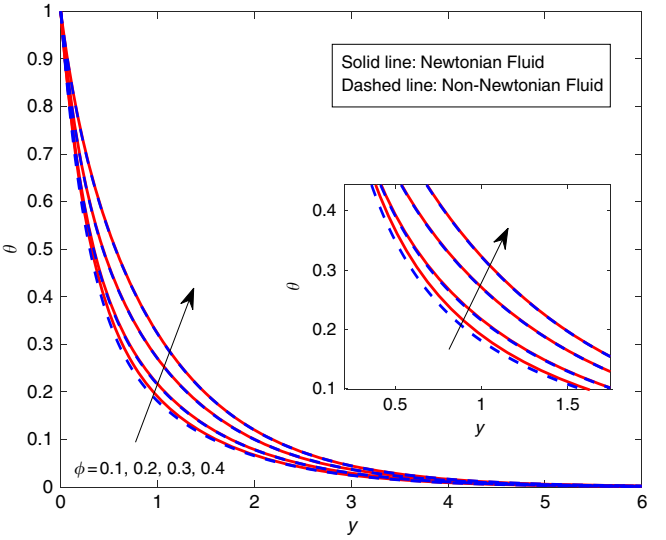

Figure 3.
Effect of φ on temperature distributions for $R_d = 3$; $Gt = 4.0$; $Gc = 2.0$; $Q_0 = 2.0$; Pr = 0.7; $Sc = 0.6$; $Ec = 0.01$; $\xi = 0.5$; $K_r = 0.1$; $K = 0.5$; $Q_1 = 2.0$

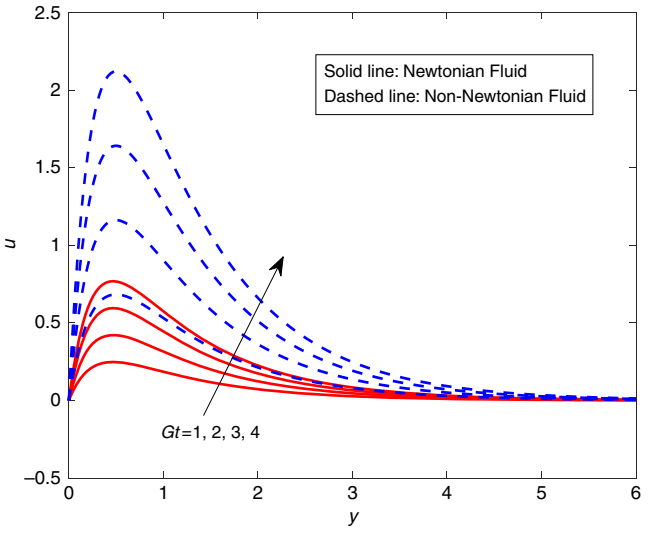

Figure 4.
Effect of Gt on velocity distributions for $R_d = 3$; $Gc = 2.0$; $Q_0 = 2.0$; $Q_1 = 2.0$; $\Pr = 0.7$; $Sc = 0.6$; $Ec = 0.01$; $\varphi = 0.05$; $\xi = 0.5$; $K_r = 0.1$; $K = 0.5$

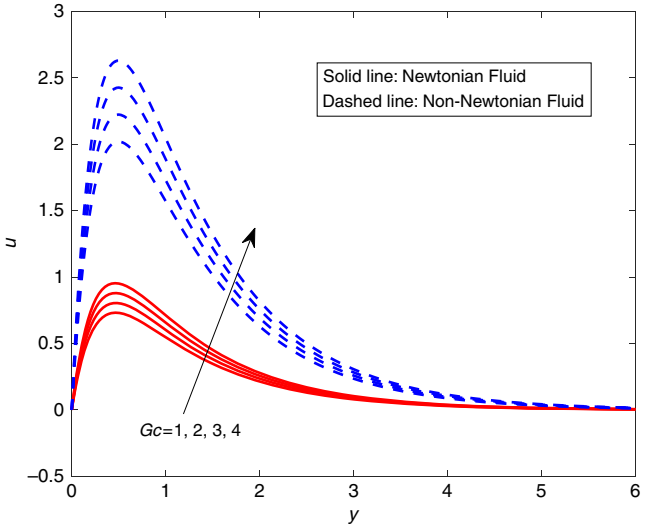

Figure 5.
Effect of Gc on velocity distributions for $R_d = 3$; $Gt = 4.0$; $Q_0 = 2.0$; $Q_1 = 2.0$; $\Pr = 0.7$; $Sc = 0.6$; $Ec = 0.01$; $\varphi = 0.05$; $\xi = 0.5$; $K_r = 0.1$; $K = 0.5$

It is perceived that the momentum boundary layer widens with mounting values of thermal and concentration Grashof numbers. Physically, escalating value of Grashof number establishes a buoyancy force which has the proficiency to boosts the interior molecular movements due to this we found enlargement in momentum boundary layers. It is interesting to mention that Casson fluid is highly influenced by these parameters as compared with the Newtonian fluid.

Nature of velocity and temperature distributions under the effect of Prandtl number revealed in Figures 6 and 7. It perceived that momentum and thermal attributes decelarates by ascending values of Prandtl number. Generally, an upsurge in Prandtl number amplifies

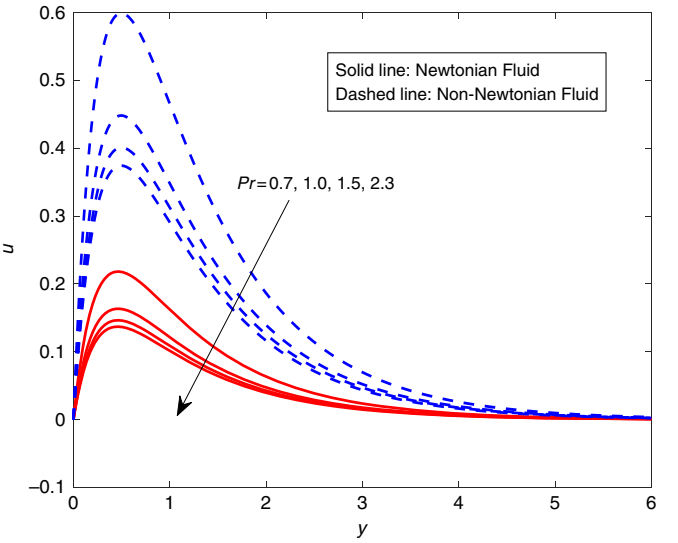

Figure 6.
Effect of Pr on velocity distributions for $R_d = 3$; $Gt = 4.0$; $Gc = 2.0$; $Q_0 = 2.0$; $Q_1 = 2.0$; $Sc = 0.6$; $Ec = 0.01$; $\varphi = 0.05$; $\xi = 0.5$; $K_r = 0.1$; $K = 0.5$

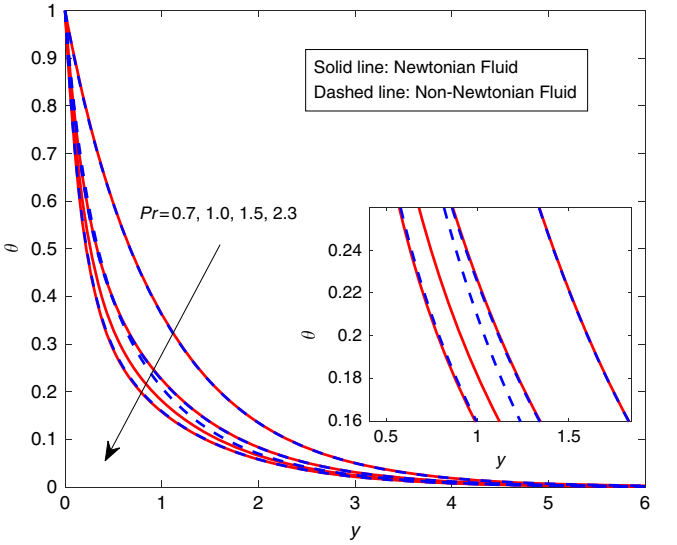

Figure 7.
Effect of Pr on temperature distributions for $R_d = 3$; $Gt = 4.0$; $Gc = 2.0$; $Q_0 = 2.0$; $Sc = 0.6$; $Ec = 0.01$; $\varphi = 0.05$; $\xi = 0.5$; $K_r = 0.1$; $K = 0.5$; $Q_1 = 2.0$

kinematic viscosity and curtails thermal diffusivity; therefore we have seen deteriorating profiles of velocity and thermal fields. Influence of thermal radiation on velocity and thermal attributes are illustrated in Figures 8 and 9. It is apparent that velocity and thermal field has contractions for escalating values of thermal radiation. Generally, raise in radiation parameter supplies heat energy to the flow, owing to this we noticed shrinkage in the momentum and thermal boundary layers.

Behaviour of velocity and concentration fields under the effect of chemical reaction parameters are portrayed in Figures 10 and 11, respectively. It witnessed that velocity and

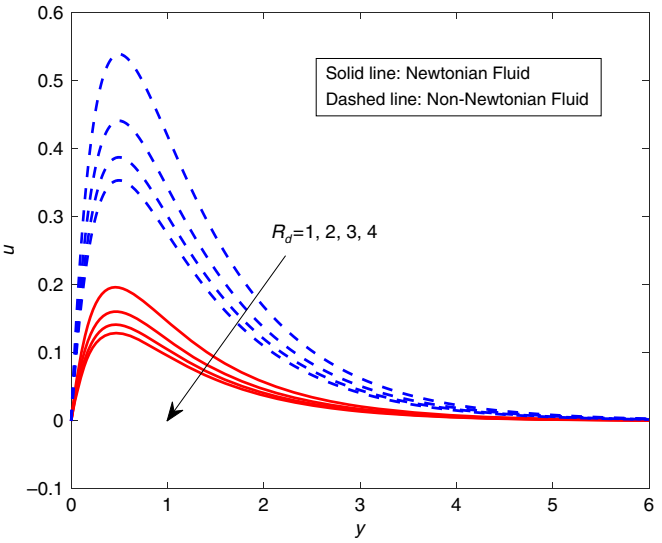

Figure 8.
Effect of R_d on velocity distributions for $Gt = 4.0$; $Gc = 2.0$; $Q_0 = 2.0$; $Q_1 = 2.0$; $\Pr = 0.7$; $Sc = 0.6$; $Ec = 0.01$; $\varphi = 0.05$; $\xi = 0.5$; $K_r = 0.1$; $K = 0.5$

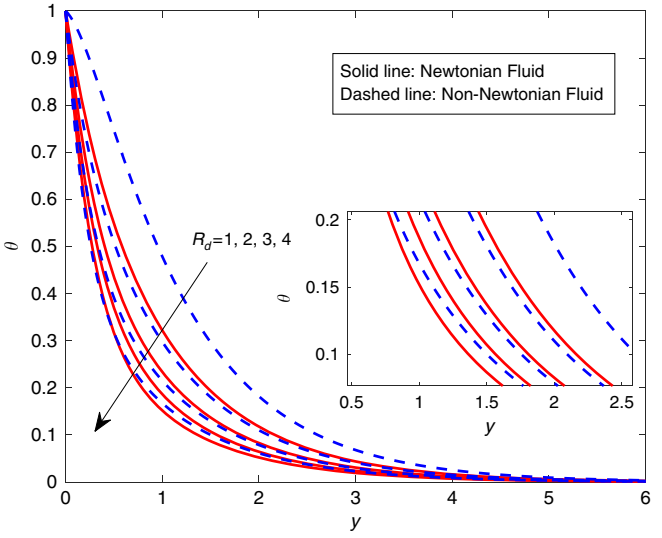

Figure 9.
Effect of R_d on temperature distributions for $Gt = 4.0$; $Gc = 2.0$; $Q_0 = 2.0$; $Q_1 = 2.0$; $\Pr = 0.7$; $Sc = 0.6$; $Ec = 0.01$; $\varphi = 0.05$; $\xi = 0.5$; $K_r = 0.1$; $K = 0.5$

concentration profiles decaying functions of amassed values of chemical reaction parameter. Physically, molecular diffusivity is diminished for regulating values of chemical reaction parameter, because of this we noticed deflation in velocity and concentration profiles. Figures 12 and 13 are exposed to spot the impact of heat source/sink and radiation absorption parameter on thermal fields. It is clear that thermal fields are upsurges by mounting the values of both heat source/sink and radiation absorption parameters. Figures 14 and 15 drawn to explore the impact of thermal Grashof number and porosity parameter on the skin friction factor. It is evident that, rising values of Gt and K the skin friction factor upsurges.

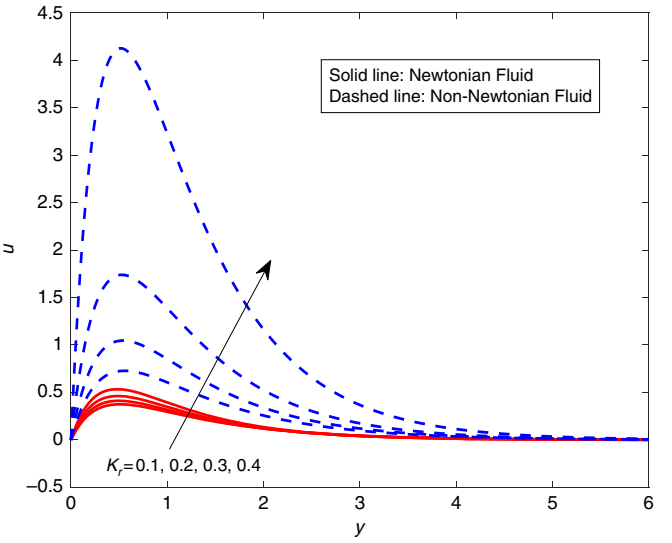

Figure 10.
Effect of K_r on velocity distributions for $R_d = 3$; $Gt = 4.0$; $Gc = 2.0$; $Q_0 = 2.0$; $Q_1 = 2.0$; $\mathrm{Pr} = 0.7$; $Sc = 0.6$; $Ec = 0.01$; $\varphi = 0.05$; $\xi = 0.5$; $K = 0.5$

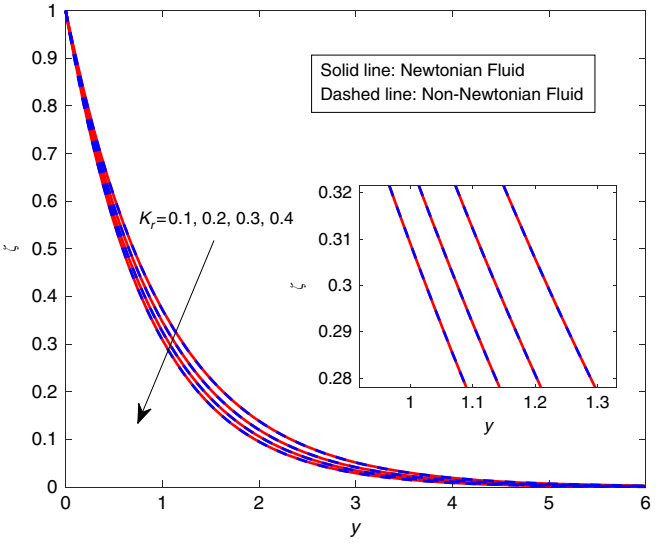

Figure 11.
Effect of K_r on concentration distributions for $R_d = 3$; $Gt = 4.0$; $Gc = 2.0$; $Q_0 = 2.0$; $\mathrm{Pr} = 0.7$; $Sc = 0.6$; $Q_1 = 2.0$; $Ec = 0.01$; $\varphi = 0.05$; $\xi = 0.5$; $K = 0.5$

Table I deployed to present the thermo-physical properties of $Al_{50}Cu_{50}$ alloy nanoparticles and base fluid at 300 K. Tables II and III predict the impact of various dimensionless parameters vs friction factor, local Nusselt and Sherwood number for both the Newtonian and non-Newtonian fluid cases. The flow rate is being decreased with amassed values of the volume fraction of nanoparticles, also we may observe Casson fluid achieves the highest peak as compared with the Newtonian fluid. An opposing trend is observed in heat transfer rate by developing values of volume fraction, radiation, and heat source/sink parameter. Also, Sherwood number is increased by taking amassed

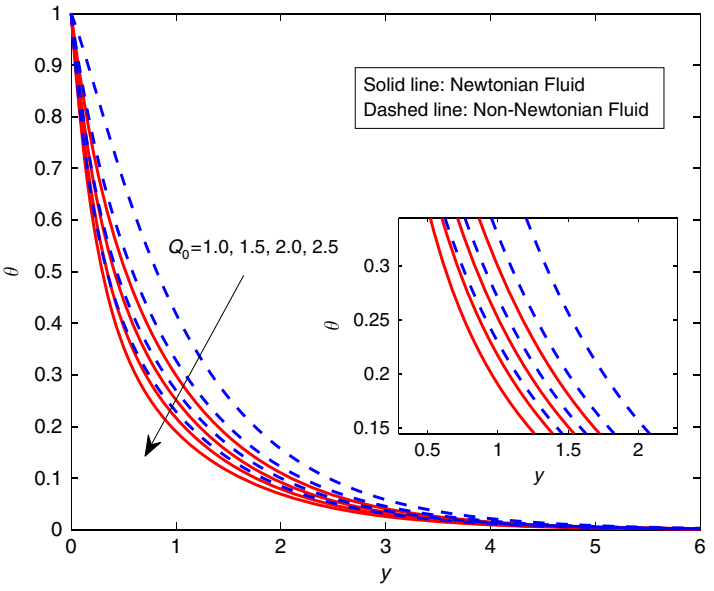

Figure 12.
Effect Q_0 on temperature distributions for $R_d = 3$; $Gt = 4.0$; $Gc = 2.0$; $Q_1 = 2.0$; $\Pr = 0.7$; $Sc = 0.6$; $Ec = 0.01$; $\varphi = 0.05$; $\xi = 0.5$; $K_r = 0.1$; $K = 0.5$

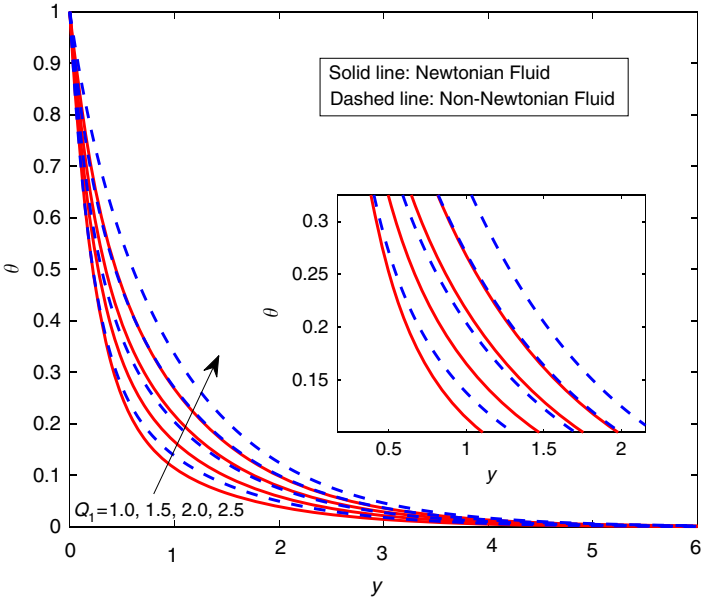

Figure 13.
Effect of Q_1 on temperature distributions for $R_d = 3$; $Gt = 4.0$; $Gc = 2.0$; $Q_0 = 2.0$; $\Pr = 0.7$; $Sc = 0.6$; $Ec = 0.01$; $\varphi = 0.05$; $\xi = 0.5$; $K_r = 0.1$; $K = 0.5$

values of chemical reaction and Schmidt number. Casson (non-Newtonian) fluid possess larger velocities and thermal transport nature as compared with Newtonian fluids. Table IV is constructed to notice the comparison between the published results with the present study results and they are in good agreement with the previous results at certain circumstances.

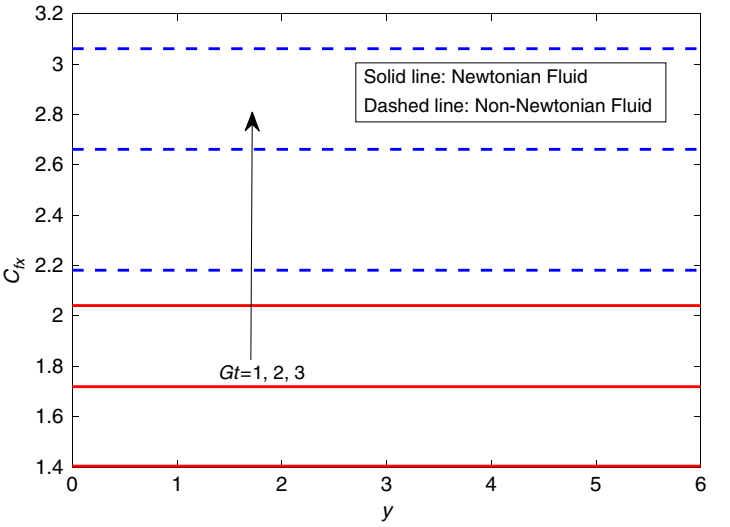

Figure 14.
Effect of thermal Grashof number Gt on Shin friction factor C_{fx} for $R_d = 3$; $Gc = 2.0$; $Q_0 = 2.0$; $Q_1 = 2.0$; Pr = 0.7; $Sc = 0.6$; $Ec = 0.01$;$\varphi = 0.05$; $\xi = 0.5$;$K_r = 0.1$; $K = 0.5$

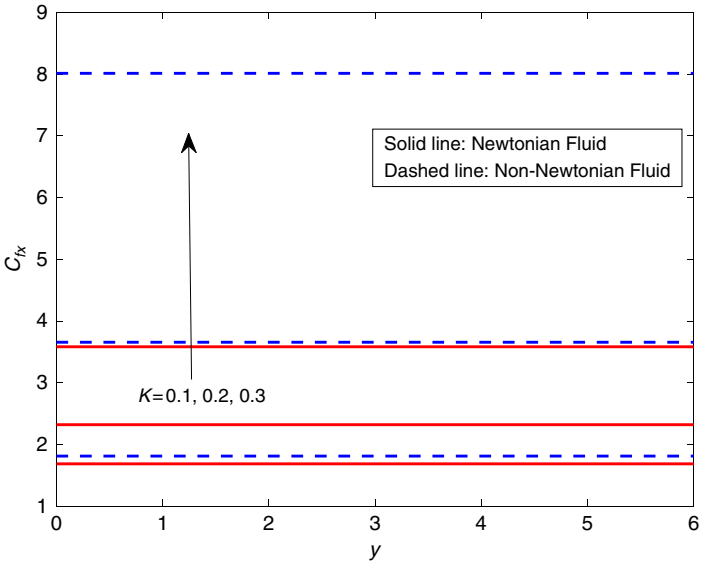

Figure 15.
Effect of porosity parameter K on Shin friction factor $C_{fx}R_d = 3$; $Gc = 2.0$; $Q_0 = 2.0$; $Q_1 = 2.0$; Pr = 0.7; $Sc = 0.6$; $Ec = 0.01$; $\varphi = 0.05$; $\xi = 0.5$; $K_r = 0.1$; $Gt = 4.0$

Physical properties	$Al_{50}Cu_{50}$	Water
c_p(J/KgK)	747.90	4,179
ρ(Kg/m^3)	4,133.68	997.3
k(W/mK)	112	0.613
σ(S/m)	1.4993×10^7	0.05

Table I.
Thermophysical properties of base fluid (Water) and alloy nanoparticles at 300K

Gt	Gc	φ	R_d	Q_0	Q_1	Sc	K_r	K	Newtonian Fluid $u'(0)$	$-\theta'(0)$	$-\psi'(0)$
1									1.3984	−8.3574	−0.9873
2									1.7144	−8.3568	−0.9873
3									2.0235	−8.3561	−0.9873
	1								1.8101	−8.3566	−0.9873
	2								2.3244	−8.3553	−0.9873
	3								2.8321	−8.3536	−0.9873
		0.1							3.1181	−5.6069	−0.9873
		0.2							2.3244	−2.3553	−0.9873
		0.3							2.1437	−13.040	−0.9873
			1						3.7737	−7.4945	−0.9873
			2						2.7583	−7.8462	−0.9873
			3						2.3244	−8.3553	−0.9873
				1					2.7583	−7.8462	−0.9873
				2					2.3244	−8.3553	−0.9873
				3					2.0696	−8.8818	−0.9873
					0.5				1.5253	−8.0306	−0.9873
					1.0				1.7937	−8.1389	−0.9873
					1.5				2.0601	−8.2472	−0.9873
						0.2			2.3133	−7.9830	−0.3732
						0.4			2.1910	−8.1296	−0.6828
						0.6			2.3244	−8.3553	−0.9873
							0.1		2.3244	−8.3553	−0.9873
							0.5		3.0222	−8.7407	−1.2245
							1.0		5.1976	−9.7989	−1.4307
								0.1	1.6835	−8.3573	−0.9873
								0.2	2.3244	−8.3553	−0.9873
								0.3	3.0250	−8.3525	−0.9873

Table II. Variation in Skin friction factor, local Nusselt number and local Sherwood number under various physical parameters for the Newtonian fluid case

5. Conclusions

This analysis reports the impact of radiation absorption and buoyancy force on the flow of Casson nanofluid past vertical surface embedded in a porous medium filled with $Al_{50}Cu_{50}$ alloy nanoparticles. Perturbation solution is acquired for the flow governing equations. Dual nature is noticed for Newtonian and non-Newtonian nanofluid cases. The significant outcomes of the present exploration are given below:

- radiation absorption parameter has the tendency to upsurge the flow rate and curtails the heat transfer rate, a reverse trend has been procured for heat source parameter;
- thermal transport nature of Casson fluid is massive as compared with the Newtonian fluid;
- nanoparticle size and shape reserved an important role in heat transfer;
- growing the thermal and concentric Grashof number progresses boundary layer thickness to raise the velocity of the flow;
- Schmidt number has a propensity to augment the amount of flow, heat and mass transfer rates;
- Casson fluid plays a vital role in enhancing the fluid velocity and thermal transport characteristics; and
- $Al_{50}Cu_{50}$ alloy nanoparticle helps in thermal conduction process.

									Non-Newtonian Fluid		
Gt	Gc	φ	R_d	Q_0	Q_1	Sc	K_r	K	$u'(0)$	$-\theta'(0)$	$-\psi'(0)$
1									2.1812	−16.0531	−0.9873
2									2.6719	−16.0492	−0.9873
3									2.6719	−16.0445	−0.9873
	1								2.8086	−16.0481	−0.9873
	2								3.6522	−16.0391	−0.9873
	3								4.4953	−16.0276	−0.9873
		0.1							3.7093	−10.5089	−0.9873
		0.2							3.6522	−16.0391	−0.9873
		0.3							3.7470	−25.2878	−0.9873
			1						6.1029	−13.7241	−0.9873
			2						4.3895	−14.8520	−0.9873
			3						3.6522	−16.0391	−0.9873
				1					4.3895	−14.8520	−0.9873
				2					3.6522	−16.0391	−0.9873
				3					3.2401	−17.1734	−0.9873
					0.5				2.2591	−15.7263	−0.9873
					1.0				2.7236	−15.8313	−0.9873
					1.5				3.1879	−15.9356	−0.9873
						0.2			2.0148	−15.6850	−0.3732
						0.4			2.2194	−15.8351	−0.6828
						0.6			3.6522	−16.0391	−0.9873
							0.1		3.6522	−16.0391	−0.9873
							0.5		25.9031	−15.7836	−1.2245
							1.0		−6.5908	−17.4761	−1.4307
								0.1	1.8198	−16.0567	−0.9873
								0.2	3.6522	−16.0391	−0.9873
								0.3	8.0143	−15.9398	−0.9873

Table III.
Variation in Skin friction factor, local Nusselt number and local Sherwood number under various physical parameters for the non-Newtonian fluid case

	Pal and Talukdar (2010)			Present results ($K = \infty$, $\Phi = 0.0$, $K_r = 0.0$)		
R_d	C_{fx}	Nu_x/Re_x	Sh_x/Re_x	C_{fx}	Nu_x/Re_x	Sh_x/Re_x
1.0	1.6362	1.2515	−0.6000	1.6362	1.2515	−0.6000
2.0	1.5620	1.5800	−0.6000	1.5620	1.5800	−0.6000
3.0	1.5137	1.8376	−0.6000	1.5137	1.8376	−0.6000
4.0	1.4781	2.0568	−0.6000	1.4781	2.0568	−0.6000
5.0	1.4499	2.2508	−0.6000	1.4499	2.2508	−0.6000

Notes: $Gt = 4.0$; $Gc = 2.0$; $Q_0 = 2.0$; $Q_1 = 2.0$; $\mathrm{Pr} = 0.7$; $Sc = 0.6$; $Ec = 0.01$; $\xi = 0.5$

Table IV.
Comparison of present results with those of Pal and Talukdar (2010) with different values of R_d for Skin friction factor, local Nusselt and Sherwood number

References

Babu, M.J. and Sandeep, N. (2016), "Three-dimensional MHD slip flow of nanofluids over a slendering stretching sheet with thermophoresis and Brownian motion effects", *Advanced Powder Technology*, Vol. 27 No. 5, pp. 2039-2050.

Babu, M.J., Sandeep, N., Ali, M.E. and Nuhait, A.O. (2017), "Magnetohydrodynamic dissipative flow across the slendering stretching sheet with temperature dependent variable viscosity", *Results in Physics*, Vol. 7 No. 1, pp. 1801-1807.

Buongiorno, J. (2006), "Convective transport in nanofluids", *Journal of Heat Transfer*, Vol. 128 No. 3, pp. 240-250.

Choi, S.U.S. (1995), "Enhancing thermal conductivity of fluids with nanoparticles", FED-231/MD-66, Developments and Applications of Non-Newtonian Flows, Argonne National Laboratory, Argonne, pp. 99-105.

Daniel, Y.S. (2017), "MHD laminar flows and heat transfer adjacent to permeable stretching sheets with partial slip condition", *Journal of Advanced Mechanical Engineering*, Vol. 4 No. 1, pp. 1-5.

Daniel, Y.S., Aziz, Z.A., Ismail, Z. and Salah, F. (2017a), "Effects of thermal radiation, viscous and Joule heating on electrical MHD nanofluid with double stratification", *Chinese Journal of Physics*, Vol. 55 No. 3, pp. 630-651.

Daniel, Y.S., Aziz, Z.A., Ismail, Z. and Salah, F. (2017b), "Impact of thermal radiation on electrical MHD flow of nanofluid over nonlinear stretching sheet with variable thickness", *Alexandria Engineering Journal* (in press), available at: https://doi.org/10.1016/j.aej.2017.07.007

Daniel, Y.S., Aziz, Z.A., Ismail, Z. and Salah, F. (2017c), "Thermal radiation on unsteady electrical MHD flow of nanofluid over stretching sheet with chemical reaction", *Journal of King Saud University-Science* (in press), available at: https://doi.org/10.1016/j.jksus.2017.10.002

Daniel, Y.S. and Daniel, S.K. (2015), "Effects of buoyancy and thermal radiation on MHD flow over a stretching porous sheet using homotopy analysis method", *Alexandria Engineering Journal*, Vol. 54 No. 3, pp. 705-712.

Dogonchi, A.S. and Ganji, D.D. (2016a), "Investigation of MHD nanofluid flow and heat transfer in a stretching/shrinking convergent/divergent channel considering thermal radiation", *Journal of Molecular Liquids*, Vol. 220 No. 1, pp. 592-603, doi: 10.1016/j.molliq.2016.05.022.

Dogonchi, A.S. and Ganji, D.D. (2016b), "Study of nanofluid flow and heat transfer between non-parallel stretching walls considering Brownian motion", *Journal of the Taiwan Institute of Chemical Engineers*, Vol. 69 No. 1, pp. 1-13, doi: 10.1016/j.jtice.2016.09.029.

Dogonchi, A.S. and Ganji, D.D. (2016c), "Thermal radiation effect on the Nano-fluid buoyancy flow and heat transfer over a stretching sheet considering Brownian motion", *Journal of Molecular Liquids*, Vol. 223 No. 1, pp. 521-527, doi: 10.1016/j.molliq.2016.08.090.

Dogonchi, A.S. and Ganji, D.D. (2017a), "Analytical solution and heat transfer of two-phase nanofluid flow between non-parallel walls considering Joule heating effect", *Powder Technology*, Vol. 318 No. 1, pp. 390-400, doi: 10.1016/j.powtec.2017.06.018.

Dogonchi, A.S. and Ganji, D.D. (2017b), "Impact of Cattaneo-Christov heat flux on MHD nanofluid flow and heat transfer between parallel plates considering thermal radiation effect", *Journal of the Taiwan Institute of Chemical Engineers*, Vol. 80 No. 1, pp. 52-63, doi: 10.1016/j.jtice.2017.08.005.

Ibrahim, W. and Makinde, O.D. (2015), "Magnetohydrodynamic stagnation point flow and heat transfer of Casson nanofluid past a stretching sheet with slip and convective boundary condition", *Journal of Aerospace Engineering*, Vol. 29 No. 2, pp. 1-11.

Ibrahim, W. and Shankar, B. (2013), "MHD boundary layer flow and heat transfer of a nanofluid past a permeable stretching sheet with velocity, thermal and solutal slip boundary conditions", *Computers & Fluids*, Vol. 75 No. 1, pp. 1-10.

Kumaran, G. and Sandeep, N. (2017), "Thermophoresis and Brownian moment effects on parabolic flow of MHD Casson and Williamson fluids with cross diffusion", *Journal of Molecular Liquids*, Vol. 233 No. 1, pp. 262-269.

Madhu, M. and Kishan, N. (2015), "Magnetohydrodynamic mixed convection stagnation-point flow of a power-law non-Newtonian nanofluid towards a stretching surface with radiation and heat source/sink", *Journal of Fluids Engineering*, Vol. 2015 No. 1, pp. 1-14.

Mahdy, A. (2016), "Unsteady MHD slip flow of a non-Newtonian Casson fluid due to stretching sheet with suction or blowing effect", *Journal of Applied Fluid Mechanics*, Vol. 9 No. 2, pp. 785-793.

Mukhopadhyay, S. (2013), "Casson fluid flow and heat transfer over a nonlinearly stretching surface", *Chinese Physics B*, Vol. 22 No. 7, pp. 1-5.

Nield, D.A. and Kuznetsov, A.V. (2009), "The ChengeMinkowycz problem for natural convective boundary-layer flow in a porous medium saturated by a nanofluid", *International Journal of Heat and Mass Transfer*, Vol. 52 Nos 25/26, pp. 5792-5795.

Pal, D. and Talukdar, B. (2010), "Buoyancy and chemical reaction effects on MHD mixed convection heat and mass transfer in a porous medium with thermal radiation and Ohmic heating", *Communications in Nonlinear Science and Numerical Simulation*, Vol. 15 No. 10, pp. 2878-2893.

Pham, TV and Mitsoulis, E. (1994), "Entry and exit flows of Casson fluids", *Canadian Journal of Chemical Engineering*, Vol. 72 No. 6, pp. 1080-1084.

Pramanik, S. (2014), "Casson fluid flow and heat transfer past an exponentially porous stretching surface in presence of thermal radiation", *Ain Shams Engineering Journal*, Vol. 5 No. 1, pp. 205-212.

Raju, C.S.K. and Sandeep, N. (2016), "A comparative study on heat and mass transfer of the Blasius and Falkner-Skan flow of a bio-convective Casson fluid past a wedge", *The European Physical Journal Plus*, Vol. 131 No. 11, p. 405, 10.1140/epjp/i2016-16405-y, doi.

Raju, C.S.K. and Sandeep, N. (2017), "Unsteady Casson nanofluid flow over a rotating cone in a rotating frame filled with ferrous nanoparticles: a numerical study", *Journal of Magnetism and Magnetic Materials*, Vol. 421 No. 1, pp. 216-224.

Raju, C.S.K., Sandeep, N., Jayachandra Babu, M. and Sugunamma, V. (2016), "Dual solutions for three-dimensional MHD flow of a nanofluid over a nonlinearly permeable stretching sheet", *Alexandria Engineering Journal*, Vol. 55 No. 1, pp. 151-162.

Sandeep, N. and Sulochana, C. (2016), "MHD flow of dusty nanofluid over a stretching surface with volume fraction of dust particles", *Ain Shams Engineering Journal*, Vol. 7 No. 2, pp. 709-716.

Shehzad, S.A., Hayat, T., Qasim, M. and Asghar, S. (2013), "Effects of mass transfer on MHD flow of Casson fluid with chemical reaction and suction", *Brazilian Journal of Chemical Engineering*, Vol. 30 No. 1, pp. 187-195.

Sulochana, C., Ashwinkumar, G.P. and Sandeep, N. (2016), "Transpiration effect on stagnation-point flow of a Carreau nanofluid in the presence of thermophoresis and Brownian motion", *Alexandria Engineering Journal*, Vol. 55 No. 2, pp. 1151-1157.

Sulochana, C., Ashwinkumar, G.P. and Sandeep, N. (2017a), "Boundary layer analysis of persistent moving horizontal needle in magnetohydrodynamic ferrofluid: a numerical study", *Alexandria Engineering Journal* (in press), doi:10.1016/j.aej.2017.08.020.

Sulochana, C., Ashwinkumar, G.P. and Sandeep, N. (2017b), "Effect of frictional heating on mixed convection flow of chemically reacting radiative Casson nanofluid over an inclined porous plate", *Alexandria Engineering Journal* (in press), doi:10.1016/j.aej.2017.08.006.

Sulochana, C., Ashwinkumar, G.P. and Sandeep, N. (2017c), "Effect of thermophoresis and Brownian moment on 2D MHD nanofluid flow over an elongated sheet", *Defect and Diffusion Forum*, Vol. 377 No. 1, pp. 111-126.

Sulochana, C., Ashwinkumar, G.P. and Sandeep, N. (2017d), "Joule heating effect on a continuously moving thin needle in MHD Sakiadis flow with thermophoresis and Brownian moment", *The European Physical Journal Plus*, Vol. 132 No. 9, pp. 387-400.

Tso, CP, Francisca, JS and Hung, YM (2010), "Viscous dissipation effects of power-law fluid flow within parallel plates with constant heat fluxes", *The Journal of Non-Newtonian Fluid Mechanics*, Vol. 165 Nos 11/12, pp. 625-630.

Vajravelu, K., Prasad, K.V, Lee, J., Lee, C., Pop, I. and Van Gorder, R.A. (2011), "Convective heat transfer in the flow of viscous Ag-water and Cu-water nano fluids over a stretching surface", *The International Journal of Thermal Sciences*, Vol. 50 No. 5, pp. 843-851.

Wang, C. and Pop, I. (2006), "Analysis of the flow of a power-law fluid film on an unsteady stretching surface by means of homotopy analysis method", *The Journal of Non-Newtonian Fluid Mechanics*, Vol. 138 Nos 2/3, pp. 161-172.

Corresponding author
Sulochana C. can be contacted at: maths.sulochana@gug.ac.in